16th World Conference on Earthquake Engineering, 16WCEE 2017
Santiago Chile, January 9th to 13th 2017
Paper N°3253
Registration Code: SM1463161930-

CONTROLLED ROCKING HEAVY TIMBER WALLS FOR REGIONS OF LOW TO MODERATE SEISMICITY

M. Kovacs[(1)], L. Wiebe[(2)]

[(1)] *M.A.Sc. Candidate, McMaster University, kovacsma@mcmaster.ca*
[(2)] *Assistant Professor, Civil Engineering, McMaster University, wiebel@mcmaster.ca*

Abstract

Controlled rocking heavy timber walls (CRHTW) have been developed and implemented in New Zealand using Prestressed-Laminated (Pres-Lam) timber products to resist large seismic loads and minimize structural damage. Controlled rocking walls are designed to rock on their foundation in response to seismic loads, and this rocking behaviour is controlled with post-tensioning (PT) and supplemental energy dissipation. The CRHTW offers environmental and economic benefits that could also be realized in lower seismic hazard regions like Eastern North America and Europe. For these regions, the reduction or omission of PT or energy dissipating elements could simplify design and construction, and the application of Cross-Laminated Timber (CLT) could increase the appeal of this structural alternative. However, the performance of such a simplified CRHTW made of CLT has not previously been evaluated. Furthermore, although previous CRHTW studies have shown that higher mode effects can increase the shear and moment demands above the design levels, these higher mode effects have not been studied for CLT CRHTW without supplemental energy dissipation. This paper addresses these questions by first presenting the design and analysis of a prototype simplified CRHTW, considering the low-to-moderate seismic hazard of Ottawa, Canada. The design process considers capacity design of the CRHTW by applying two recently-proposed methods for estimating higher mode effects. A numerical model of the design is developed and subjected to non-linear time history analyses (NLTHA) with twelve ground motions that are representative of the design hazard with a 2% probability of exceedance in 50 years. The NLTHA results show that, despite the omission of supplemental energy dissipation, the wall's peak displacements are only 0.63% of the wall height, interstorey drifts are significantly below the 2.5% limit, and the maximum shear and bending moment demands are 45% and 70% of capacity, respectively. Of the two methods considered for predicting the peak forces caused by higher mode effects, one is accurate to within 30% and the other to within 15%, both without any empirical calibration.

Keywords: Cross-Laminated Timber, Low-damage Seismic Design, Controlled Rocking, Higher Mode Effects

1. Introduction

High risk regions, in which large populations are vulnerable to the effects of high seismic hazards, have adopted advanced technologies like damping devices, base isolation, and controlled rocking, to mitigate risk due to seismic events. However, risk is not only a function of hazard: low-to-moderate seismic hazard regions face similarly high risks as urban population centers densify, especially by building upward to accommodate growing populations and economies [1]. Additionally, a low perception of seismic risk in regions of low-to-moderate seismicity results in opposition to seismic resistant structural alternatives that are considered complex and expensive [2]. One way for structural engineers to overcome this challenge is to simplify solutions that have been developed for greater seismic hazards, and to combine these solutions with other features desired by stakeholders. For example, the Government of Canada has identified Cross-Laminated Timber (CLT) as an environmentally and economically advantageous construction material for both Canada and the U.S. [3], and several CLT systems are being studied for high seismic hazard regions [4–7]. By simplifying the design and construction of CLT systems, there is an opportunity to adapt low-damage CLT-based structural alternatives to regions of low-to-moderate seismicity.

One potential solution is a controlled rocking heavy timber wall (CRHTW) constructed of CLT and without energy dissipation. CRHTWs have been developed for regions of high seismic hazard in New Zealand, so as to control structural damage during a seismic event [5]. They are designed to rock on their foundation in response to seismic loads, with rocking initiated at a fraction of the base overturning moment (divided by force reduction factor, R_dR_o) that would develop if the wall were designed to remain linear elastic, as shown in Fig. 1.1. The rocking behaviour is controlled and the wall is returned to its original position with post-tensioning (PT) elements.

Also, supplemental energy dissipation elements are installed to reduce peak displacements and accelerations. Fig. 1.1 (a-c) depicts three variations of the CRHTW: (a) a cantilever CRHTW at rest; (b) coupled rocking walls with energy dissipating couplers and yielding steel dissipater elements at the base [8]; and (c) a simplified CRHTW without supplemental energy dissipation, designed with a relatively large R_dR_o factor. In high seismic hazard regions, variation (b) is the focus of ongoing research seeking to address PT losses due long-term loading and timber's dimensional instability, and cyclic damage to the energy dissipation elements [9,7]. These issues increase initial and long-term costs, as well as the design complexity of a CRHTW. Alternatively, the simplified CRHTW (variation (c)) could avoid these concerns by sacrificing the benefits of supplemental energy dissipation, which may not be necessary in regions of lower seismic hazard. However, research is needed to verify the performance of a CRHTW without supplemental energy dissipation, and with a relatively large R_dR_o factor.

The CRHTW is designed and analyzed considering a set of timber properties and post-tensioning loads, and assuming the first mode response dominates these demands at the base connection. However, moment and shear demands over the height of the wall are also important performance variables to consider, based on observations from testing on Laminated Veneer Lumber (LVL) CRHTWs [9,10]. Higher mode effects can increase bending moment and shear demands over the height of the structure, relative to the base connection, depending on the structural dynamic properties, and this is especially important to consider for CRHTWs designed with different timber products. In particular, CLT CRHTWs have lower bending and shear stiffness and strength properties than LVL, as shown in Table 1, thereby increasing the CLT CRHTW's susceptibility to higher mode effects. The effects could be significant, and therefore there is a need to examine higher mode effects in simplified CLT CRHTWs.

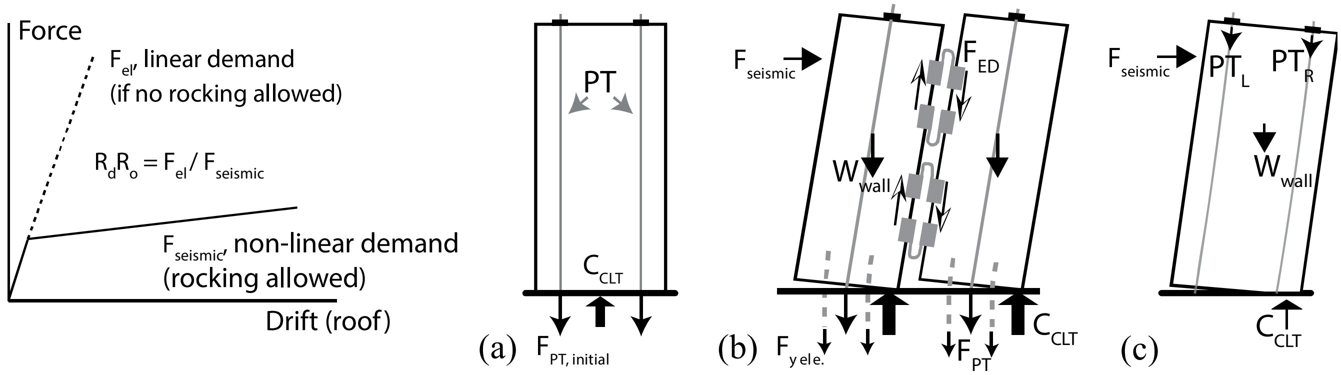

Fig. 1.1 – CRHTW force-deformation behaviour, and associated CRHTW variations (a) static state, (b) coupled, energy dissipative, (c) simplified, without energy dissipation

Table 1 – Comparing CLT and LVL design and modelling input (left), performance phenomena (right)

Property Parameter	**Difference from LVL [1]**	**Value[2] (gross section)**	**Phenomenon**	**CLT, compared to LVL**	
Comp. Strength, f_c	▼ 60-70%	13 MPa	Toe crushing	▼ f_c →	▲ Likelihood of damage
Elastic Modulus, E	▼ 40-50%	7,900 MPa	Mechano-sorptive effects	▲Dimensional stability →	▼ Impact on performance
Bending Strength, $f_{b,eff}$	▼ 50-60%	19 MPa			
Shear Strength, $f_{v,eff}$	▼ 50-75%	1.5 MPa	Forces due to higher mode effects	▼ f_b, f_v →	▲ Likelihood of strength demand governing
Shear Modulus, G	▼ 20-25%	520 MPa			

[1]Relative to LVL models [10–12]
[2]Property values approximated for 9-layer CLT panel, considering composite method for analysis [12,13]

This paper seeks to develop a better understanding of the performance of simplified CLT CRHTWs in low-to-moderate seismic hazard regions, and to evaluate the impact of higher mode effects on the system. Furthermore, this paper seeks to evaluate how higher mode effects in CRHTWs can be predicted as part of a capacity design procedure. To achieve these objectives, a prototype CRHTW is presented, and the associated analysis, design, and numerical modeling theory is discussed. Additionally, two higher mode effect estimation methods that have previously been proposed for controlled rocking steel braced frames are reviewed and applied to the prototype. Next, NLTHA results from the numerical model are investigated, with a focus on the bending and shear demands as well as the interstorey drifts, roof displacements, and floor accelerations. Finally, the accuracy of the higher mode estimation methods is evaluated.

2. Prototype: Analysis & Design

2.1 Prototype Structure

The discussion and analyses presented in this paper are associated with the following prototype building, which uses CRHTWs to resist low-to-moderate seismic hazard demands. The prototype is a six-storey, 54 m square building designed for Ottawa, a region of low-to-moderate seismic hazard in Canada [14]. Each storey is 3.3 m high, for a total height of 19.8 m. The floor weights and load combinations are summarized in Table 2. The prototype design includes twenty-four CRHTWs with the timber properties outlined in Table 1; a sample layout of the building is presented in Fig. 2.1. The CRHTW panel is a standard 2440 mm wide, 315 mm thick panel from Canada's Nordic Structures (314-9L) [12], with one 26 mm DYWIDAG PT bar [15] located 600 mm from each side of the wall. Both PT elements have an initial post-tensioning load ($T_{PT,init}$) of 83.5 kN. The following sections review the analysis and design theory that was applied to develop the prototype CLT CRHTW; further details are available in [14,16]. Additionally, capacity design is included in the design process by reviewing two methods that have been proposed to predict the higher mode effects in controlled rocking steel braced frames and applying them to the prototype CRHTW.

Table 2 – Prototype loading contributions (left); total storey weights for seismic design (right)

Roof Pressure		**Floor Pressure**		**Total Seismic Storey Weight (Dead+0.25×Snow)**	
Dead Load [17]	Snow Load [18]	Dead Load [17]	Snow	6^{th} Storey (Roof)	1^{st} – 5^{th} Storey (per storey)
2.3 kPa	2.4 kPa	3 kPa	-	8490 kN	8810 kN

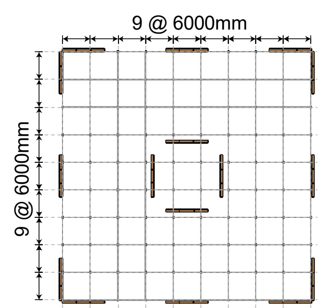

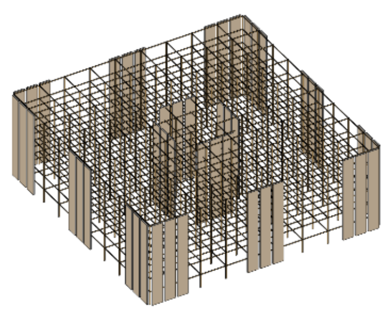

Fig. 2.1 – Sample layout with twenty-four walls

2.2 Base Mechanics Analysis

The earthquake loading imposes bending (θ_f), shear (θ_s), and rigid body (θ_{con}) deformations on the wall, as shown in Fig. 2.2 (a). θ_{con} is caused by base uplift and compression, as shown in Fig. 2.2 (b), and it results in elongation of the PT tendons, which creates an overturning moment (OTM) resistance that returns the wall to its original position. Therefore, understanding the relationship between OTM and θ_{con} (base mechanics) is important to CRHTW analysis and design. In this study, the CRHTW base mechanics are computed using the Winkler Spring Analogy (WSA) [10] in which the base is represented as a series of springs with axial stiffness, $E_{timber}A/L_{eff}$. The springs represent the base connection interface, which is evaluated as a continuous section (integrated, as in the following base mechanics analysis process), or as a finite series of springs with area, A (as in the numerical model, Section 3). L_{eff} is defined by an empirical relationship, proposed by Newcombe (Eq. (1)) [10,19]. With the WSA, the timber compression component of the OTM resistance can be determined, as in the following analysis process based on research by Newcombe [10,19] and Sarti [9]; details of the process for the simplified CRHTW are presented in [16].

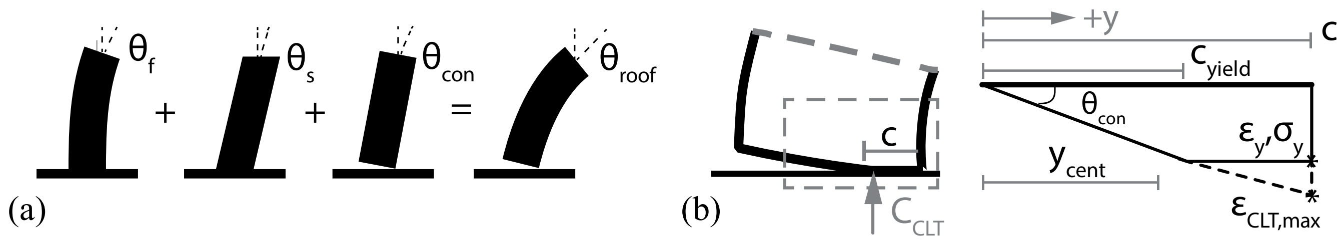

Fig. 2.2 – (a) Flexure, shear, and rigid body rotation components of CRHTW analysis; (b) result on rocking toe

First, a base connection rotation (θ_{con}) is identified for analysis (see Fig. 2.2 (b)), a corresponding neutral axis depth (c) is assumed, and the Winkler spring length (L_{eff}) is calculated as per the WSA (Eq. (1)). The c-L_{eff} relationship is significant to the analysis process, and also for numerical modeling: L_{eff} relies on c, but it is computationally expensive to solve for c at every θ_{con}. Therefore, a constant L_{eff} term is determined for which θ_{con}-c corresponds to the peak θ_{roof} value (typically 2-2.5%) [19].

$$L_{eff} = 120\left(\frac{W_w}{c}-1\right), \text{where } \mathrm{W_w} = \text{wall width} \qquad (1)$$

Next, the rocking toe interface is evaluated using the strain profile ($\varepsilon_{CLT}=\theta_{con}c/L_{eff}$) in the compressed (rocking) toe interface (Fig. 2.2 (b)) The strain profile is converted to a stress profile considering a bilinear material relationship: σ_y and c_y are the yield stress and corresponding depth from the neutral axis to the timber yield point, respectively. Given this compression interface profile, the compression force (C_{CLT}) and compression toe centroid (y_{cent}) are determined by integration.

The CRHTW PT forces are calculated next: the initial PT forces are modified by rocking as shown in Fig. 2.3. The vertical and horizontal components of the PT force are determined by considering the PT material properties and the system geometry at the given θ_{con}.

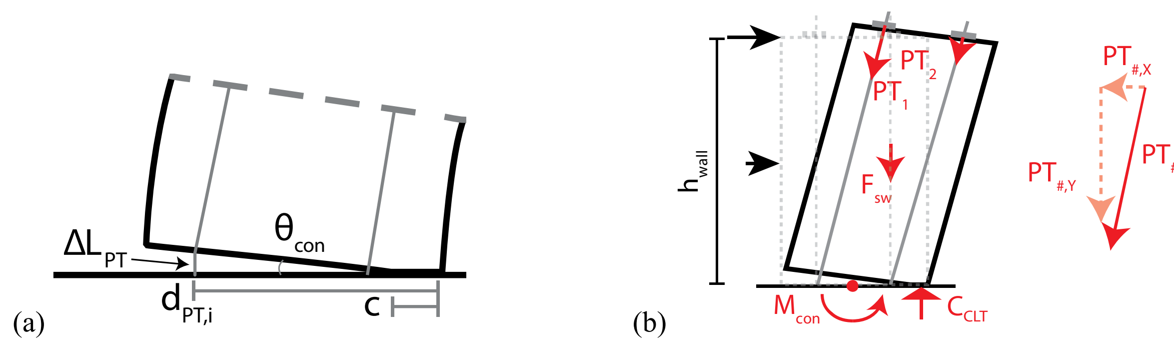

Fig. 2.3 – (a) Elongating PT due to rocking; (b) PT components and the system response

Next, force equilibrium is checked at the base connection interface, considering rocking toe compression, post-tensioning, and wall self-weight. If equilibrium is not satisfied, it is necessary to iterate the analysis with a new c.

If the base connection force equilibrium is satisfied, then the base connection moment (M_{con}) and base shear (V_b) can be calculated. M_{con} is determined from the components in Fig. 2.3 (b). In a tall CRHTW, the horizontal PT force contribution at the roof becomes significant as θ_{con} increases, so both the horizontal and vertical PT components are calculated. V_b is determined from M_{con} by dividing M_{con} by the effective height of the structure ($H_{eff}=\sum(m_ih_i^2)/\sum(m_ih_i)$).

Finally, the total roof drift is determined by considering the sum of bending and shear displacements (δ_b and δ_s respectively) over the wall height (h_w) and adding the rigid body rotation, θ_{con}. δ_b and δ_s can be determined using conventional structural mechanics. A simplified equation is provided by Sarti in [9], and further developed for the widely space PT configuration in [14].

2.3 Base Connection Design

The CRHTW design method is based on a similar design methodology from [20], but was modified for CRHTWs in [16]. Presented herein is a summary of the design method, including numerical details for the prototype design.

First, a T_n estimate is required for an initial design iteration. Research is needed to develop guidance for the initial T_n estimate, but the Rayleigh method can be applied to check the T_n assumption after an initial design has been developed. For the prototype model, T_n is 1.80 seconds, and was verified at the end of the design.

Next, both seismic and wind demands are evaluated, as wind demands may govern in low-to-moderate seismic hazard regions. For calculating the seismic demands, a force reduction factor (R_dR_o) of 8.0 was selected for design of the prototype structure. This selection was based on research that has suggested that it may be possible to control the peak displacements to within reasonable limits with R_dR_o of 8.0, even without supplemental energy dissipation [21]. With R_dR_o = 8.0, the seismic base shear demand (V_b) is determined by the equivalent static force procedure (ESFP), and is 20% lower than the base shear caused by wind [14]. However, due to the vertical distribution of seismic load, the seismic OTM demand (OTM_{design}) governs the base connection design: the seismic OTM is 6000 kN·m, compared to 5050 kN·m due to wind load.

Given OTM_{design}, the building configuration is determined, including a quantity of walls for the whole building. Next, $T_{PT,init}$ is calculated for each wall, to resist that wall's share of OTM_{design}. For the widely-spaced PT design, it is assumed that rocking is initiated when c meets the least-strained PT element as shown in Fig. 2.4 (a), and that the cumulative PT force is assumed unchanged. This assumption was found to be sufficiently accurate using the analysis process of Section 2.2. Therefore, taking the PT forces equal to the initial PT force ($T_{PT,init}$), the required $T_{PT,init}$ is determined by Fig. 2.4 (b) and Eq. (2).

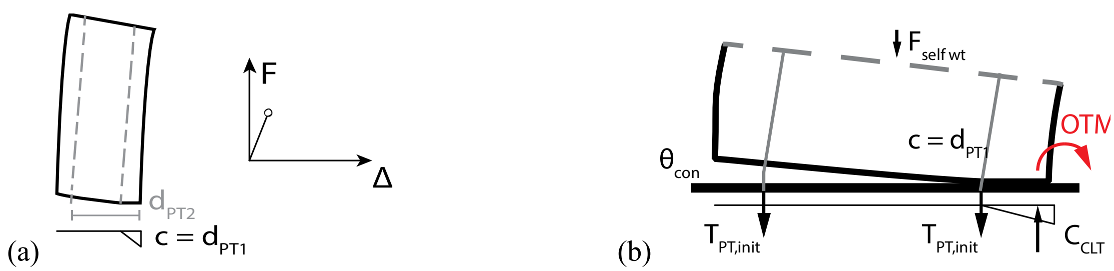

Fig. 2.4 – (a) Peak of elastic system response; (b) base connection moment at system yield, for design

$$T_{PT,init} = \frac{OTM_{design} - F_{self\ wt}\left(\frac{W_w}{2} - \frac{c}{3}\right)}{d_{PT1} + d_{PT2} - \frac{2c}{3}} \quad (2)$$

The final design step is to estimate the non-linear roof drift, $\theta^{non\text{-}lin}_{roof,design}$ and compare against peak drift limitations. $\theta^{non\text{-}lin}_{roof,design}$ due to the CRHTW design force is determined by calculating the bending and shear deflection over the wall height (h_w), as shown in the analysis process of Section 2.2. Bending and shear deflection due to the design forces correspond with Δ_y in Fig. 2.5. Δ_y is then multiplied by $C_RR_dR_o$ to estimate the total $\Delta_{non\text{-}lin}$ while rocking, where C_R is a displacement correction factor that is given in [21]; for the prototype, C_R is 2.04. $\Delta_{non\text{-}lin}$ is divided by h_w to determine $\theta^{non\text{-}lin}_{roof,design}$. For the prototype model, the estimated $\Delta_{non\text{-}lin}$ is 165 mm, equal to 0.83% roof drift. This is much less than the 2.5% drift allowance for normal importance buildings in the Canadian building code [18].

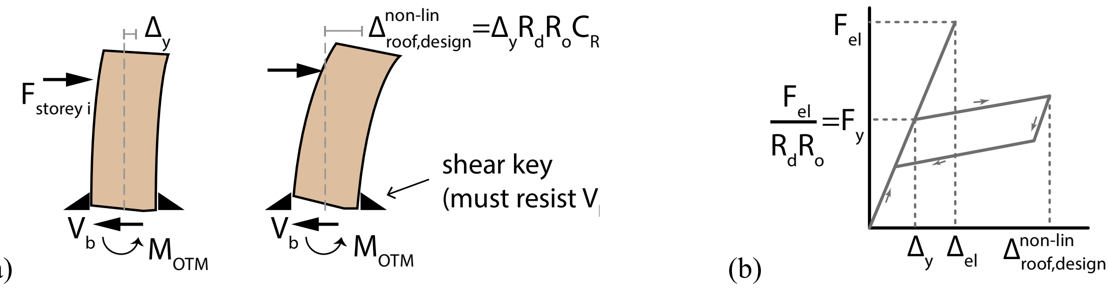

Fig. 2.5 – (a) CRHTW design forces and expected non-linear displacement; (b) CRHTW system hysteresis

2.4 Capacity Design: Considering Higher Mode Effects

Two higher mode estimation methods are considered in the work, as described in the following sections. Both methods are based on recently proposed techniques for controlled rocking steel braced frames [22]. In both methods, the first mode response contribution is calculated by multiplying the code-defined lateral forces by an overstrength factor (Ω). This factor is determined by applying the analysis process of Section 2.2 to calculate M_{con} when the roof drift is equal to $\theta^{non\text{-}lin}_{roof,design}$, determined in the wall design. Ω is defined by Eq. (3).

$$\Omega = \frac{M_{con}}{OTM_{design}} \tag{3}$$

2.4.1 Dynamic Method

The first method considered for predicting higher mode effects is the dynamic method, and it can be conducted with a model built in commercial structural engineering software [22]. Elastic wall panel elements are defined with the seismic masses at storey nodes, and rigid elements are used to connect the centerline of the wall with nodes at the PT anchorages and at the rocking toe, as shown in Fig. 2.6. The rocking toe is pin supported, and the top-of-wall PT nodes are supported by vertical springs with the axial stiffness of the PT elements; the PT nodes are statically loaded with $T_{PT,init}$. Next, a force is applied at each storey to simulate the first-mode response, i.e. the inverted-triangular load distribution from design, and Ω (defined by Eq. (3)) is applied to the lateral forces to account for the CRHTW response at $\theta^{non\text{-}lin}_{roof,design}$. In the prototype, M_{con} at $\theta^{non\text{-}lin}_{roof,design}$ (0.83%) is 450 kN·m, as shown in the pushover plot of Fig. 2.6 (b), and the design OTM (OTM_{design}) is 250 kN·m, so Ω is 1.80. The next step of the dynamic method requires a truncated response spectrum analysis, in which the design spectrum is truncated between the first- and second- mode periods so as to capture only the higher modes [22]. Finally, the truncated response spectrum analysis results are combined by the square root of the sum of the squares (SRSS) method and added to the first mode contribution including Ω, as described above. This is shown in Eq. (4), where r is the moment or shear at each node. The response spectra used in this research are presented in Section 3.2. The peak bending moment and shear demands from the dynamic method are 1,780 kN·m and 335 kN, respectively, and the distribution of moment and shear over the height is discussed in Section 4.1.

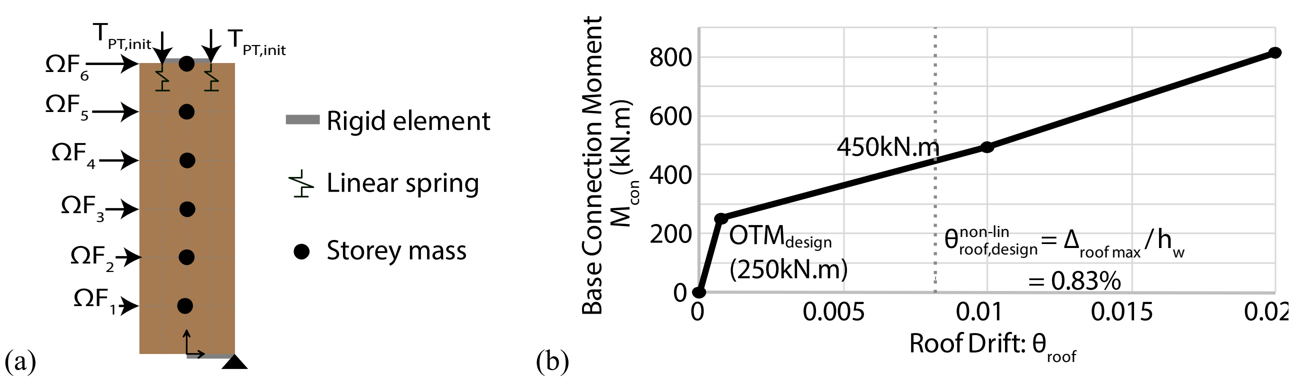

Fig. 2.6 – (a) Dynamic model diagram, and (b) pushover plot for determining Ω

$$r_{total} = r_{mode\ 1} + \sqrt{r^2_{mode\ 2} + r^2_{mode\ 3}} \tag{4}$$

2.4.2 Cantilever Beam Analogy

The cantilever beam analogy (CBA) for predicting higher mode effects involves determining the peak shear and moment response contributions from the first, second, and third modes, using closed-form equations that are given in [23]. These contributions are described by non-linear functions of the design base rocking moment (OTM_{design}), storey heights (z), total wall height (h_w), and the acceleration response spectrum at the respective higher mode periods ($S_a(T_i)$). The modal response contributions are identified as $M_{i,max}(z)$ and $V_{i,max}(z)$ for the bending moment and shear response, respectively; i refers to the mode. The $M_{i,max}(z)$ functions are shown graphically in Fig. 2.7 as an example of the shapes of these modal contributions. In the CBA, the first mode bending moment and shear contributions ($M_{1,max}(z)$ and $V_{1,max}(z)$) are calculated and amplified by Ω, as described previously. To calculate the higher mode contributions, the higher mode periods are calculated by a modal analysis. The second- and third-mode periods of the prototype are 0.36 s and 0.12 s, respectively. Next, the second- and third-mode contributions are calculated as per the respective equations in [23]. Finally, the higher mode responses are combined as per Eq. (4), where r is the $M_{i,max}(z)$ or $V_{i,max}(z)$ response from each mode, and r_{total} represents the peak total response at height, z. The peak bending moment and shear demands from the CBA are 1510 kN·m and 310 kN, respectively, and the distribution of moment and shear over the height is discussed in Section 4.1.

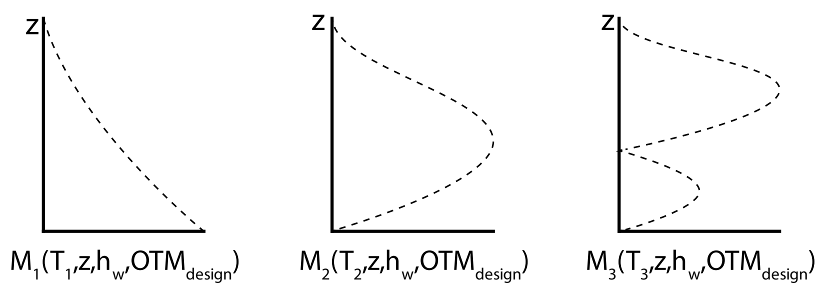

Fig. 2.7 – Non-linear modal contribution functions for peak moment response over wall height

2.4.3 Wall Demand-Capacity Ratios

The CRHTW bending capacity is defined as $M_{cap}=f_{b,eff}\cdot S$, and the shear capacity (V_{cap}) is defined as $V_{cap}=A_v\cdot f_{v,eff}$, where S is the section modulus, A_v is the shear area of the gross wall cross section, and $f_{b,eff}$ and $f_{v,eff}$ are defined in Table 1. For the prototype design, the bending moment and shear capacity are 5,900 kN·m and 960 kN, respectively; these capacities are much larger than the peak demands estimated in Sections 2.4.1 and 2.4.2. Considering the bending moment demand, the dynamic method and CBA predictions correspond to 30% and 26% of capacity, respectively, considering the shear demand, the predictions from the dynamic method and the CBA correspond to 35% and 32% of capacity, respectively. The dynamic method is more conservative in both cases.

3. Numerical Modeling

3.1 Numerical Model Development

The numerical model of the prototype structure that was constructed in OpenSees [24] is shown schematically in Fig. 3.1 (a). The model relies on the Winkler Spring Analogy (WSA) to capture the stresses in the CRHTW base. The primary wall elements are represented by elastic Timoshenko beams, capturing both shear and bending deformations. PT elements are represented by corotational truss elements with the Steel02 material model to capture the PT stress-strain relationship. Steel02 also allows for an initial PT stress, which is calibrated to achieve $T_{PT,init}$ after the model is initiated, since the wall shortens under the initial compression. Rigid elements are modelled at the top and bottom of the CRHTW to connect the wall centreline with the top of the PT elements, and also the Winkler Springs at the base, as seen in Fig. 3.1.

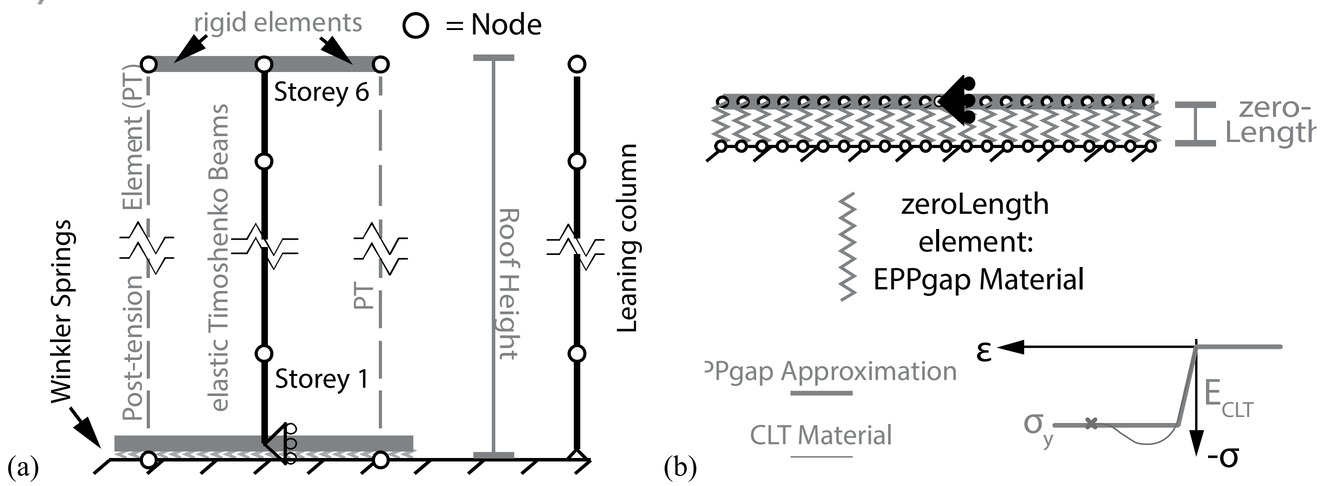

Fig. 3.1 – (a) OpenSees numerical model; (b) Base connection (Winkler Springs), including the material model

The Winkler springs, representing finite elements of the base connection, are defined by zero-length elements with an elastic perfectly plastic gap material (Fig. 3.1 (b)). This material does not have any stiffness in tension, but it has an initial compression modulus reflecting the timber material and a yield stress reflecting the CLT crushing stress. The effective length is determined from Eq. (1).

A leaning column represents the gravity system associated with the CRHTW, capturing P-Delta effects in the model. Also, a tangent-stiffness Rayleigh damping model is applied to the numerical model, with a damping ratio of 5% for the first and third modes.

3.2 Ground Motion Selection and Scaling

Twelve scaled ground motions (GMs) are used in the NLTHA. The GMs are from a synthetic set [25], and represent near- (10-25 km) and far-field (15-100km) eastern Canada M6 and M7 events (four sets of three GMs). The GMs are scaled to the Ottawa uniform hazard response spectrum, representing a 2% probability of exceedance in 50 years [18]. The range of periods considered is $0.2T_n$-$2T_n$, where T_n is 1.80 s for the final design. M6.0 events are used for scaling in the short period range ($0.2T_n – T_n$) whereas M7.0 events are scaled in the long period range ($T_n – 2T_n$), in accordance with [26]. The scaled displacement spectra are presented in Fig. 3.2. The figure confirms that the M7.0 events are more significant at long periods, which drive the first-mode response, whereas M6.0 events dominate periods shorter than 0.75 s, which are significant for higher mode effects.

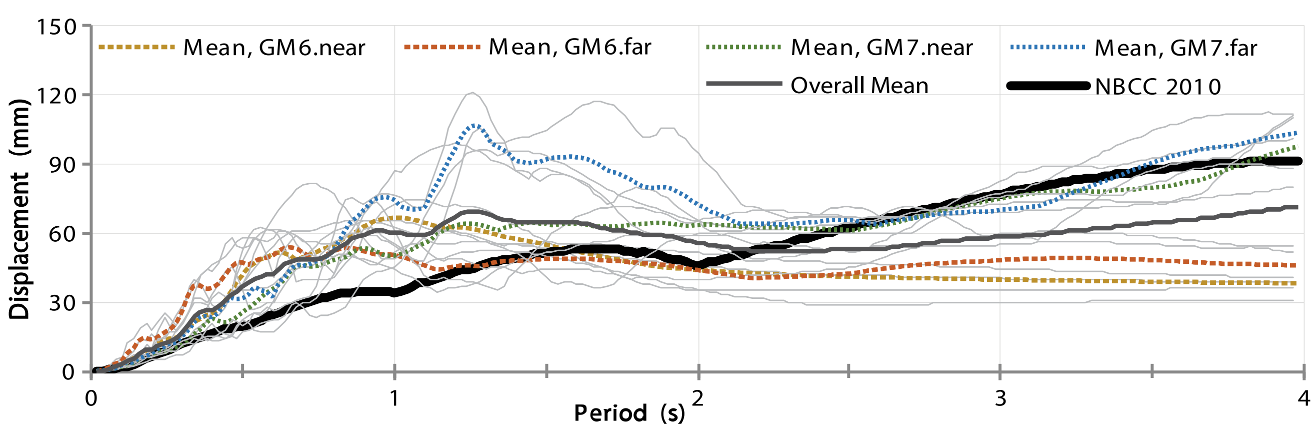

Fig. 3.2 – Scaled displacement response spectra, including mean of each set, overall mean, and design spectrum

4. NLTHA Results

Fig. 4.1 shows the CRHTW roof drift during four of the twelve time-history records, one record from each of the four sets. In the M6 events shown in Fig. 4.1 (a), high-frequency content is evident in the roof drift response during the ground motion, but the high-frequency vibration dissipates quickly as the wall continues to rock after the ground motion subsides; the peak roof drifts in these records are less than 0.5%. In contrast, the records from the M7 events shown in Fig. 4.1 (b) demonstrate larger peak roof drifts (nearly 1% in the most demanding case), and relatively little low-frequency content. All the records show that the model is initially excited to a peak displacement during the seismic event, followed by long period free vibration that dominates the response during the latter part of the earthquake and after. The records exhibit relatively little apparent interaction with the ground motions after rocking is initiated.

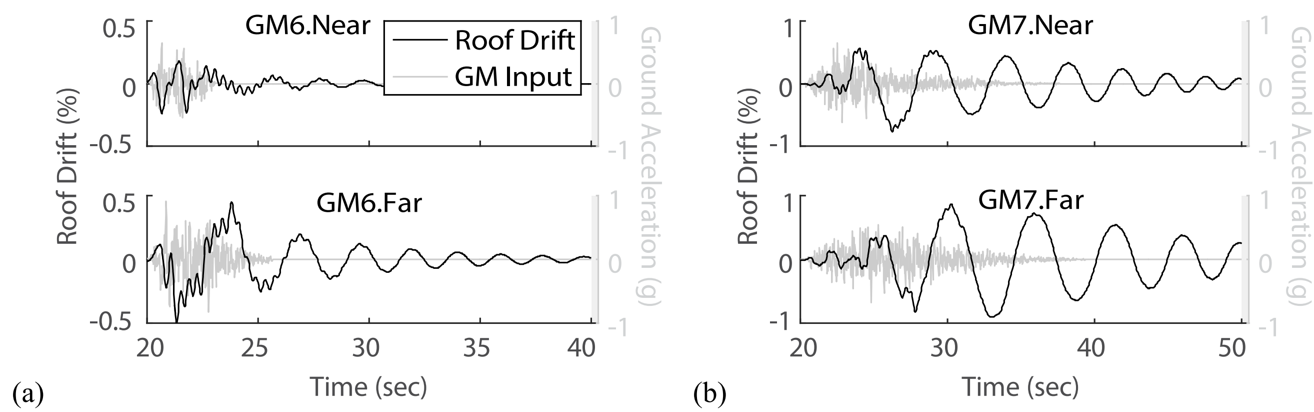

Fig. 4.1 –Roof drift time-history records from scaled GMs: (a) M6 events; (b) M7 events

Fig. 4.2 (a) shows that the interstorey drift envelopes are also lower during the M6 events than during the M7 events, but that they are also less uniform during the M6 events. This smaller but non-uniform response is due to the higher modes that are activated by the higher-frequency content of the M6 events. In contrast, the lower-frequency content of the M7 events drives a larger interstorey drift response through rigid body rocking, with limited higher mode contribution. The median peak interstorey drift responses are significantly lower than the 2.5% limit for normal importance buildings in the NBCC [18]. The peak storey displacements are not included in Fig. 4.2 (a); however, the mean peak roof displacement is 12% lower than the estimated inelastic displacement ($\Delta_{non-lin}$). The difference is likely attributable to the empirical C_R-relationship, which was calibrated for California seismic events that have more low-frequency content [21] than the Eastern Canada GMs used in the NLTHA [25].

The force demands over the wall height, shown in Fig. 4.2 (b) and (c), also reflect higher mode effects: the shear is significantly higher than the demand determined by the equivalent static force procedure applied in the wall design, which varied from 5 kN at the roof to 18 kN at the base. Similarly, the moments that occur near the wall mid-height are larger than the design base connection moment (M_{con}) of 250 kN·m. A similar influence of the modes on the peak demands has been observed in other CRHTW studies [9,10], and for controlled rocking systems in general [20]. However, the peak demand was generally observed at the base of the six-storey CRHTWs in [9,10]; therefore, Newcombe suggested that M_{con} (bending moment at the base) could be used to check the wall strength [10]. This is not conservative in this case, likely due to the relatively large R_dR_o factor, which reduces the contribution of the first mode relative to the higher modes. Nonetheless, considering the capacities determined in Section 2.4.3, the maximum peak bending and shear demand are still only 28% and 35% of capacity, respectively.

Finally, floor accelerations are considered because of their importance for acceleration-sensitive elements, such as non-structural elements anchored to the floor. Floor accelerations have been identified as a significant concern in controlled rocking systems without energy dissipation [10]. A floor acceleration limit of 1.80 g has previously been recommended for avoiding non-structural element damage [27]. Fig. 4.2 (d) shows the peak floor accelerations for the prototype model, including the median response and the 1.80 g limit. Even without supplemental energy dissipation, the floor accelerations are much less than the recommended limit. However, the higher mode effects are recognizable in Fig. 4.2 (d), with the high-frequency content of the M6 events resulting in higher peak floor accelerations.

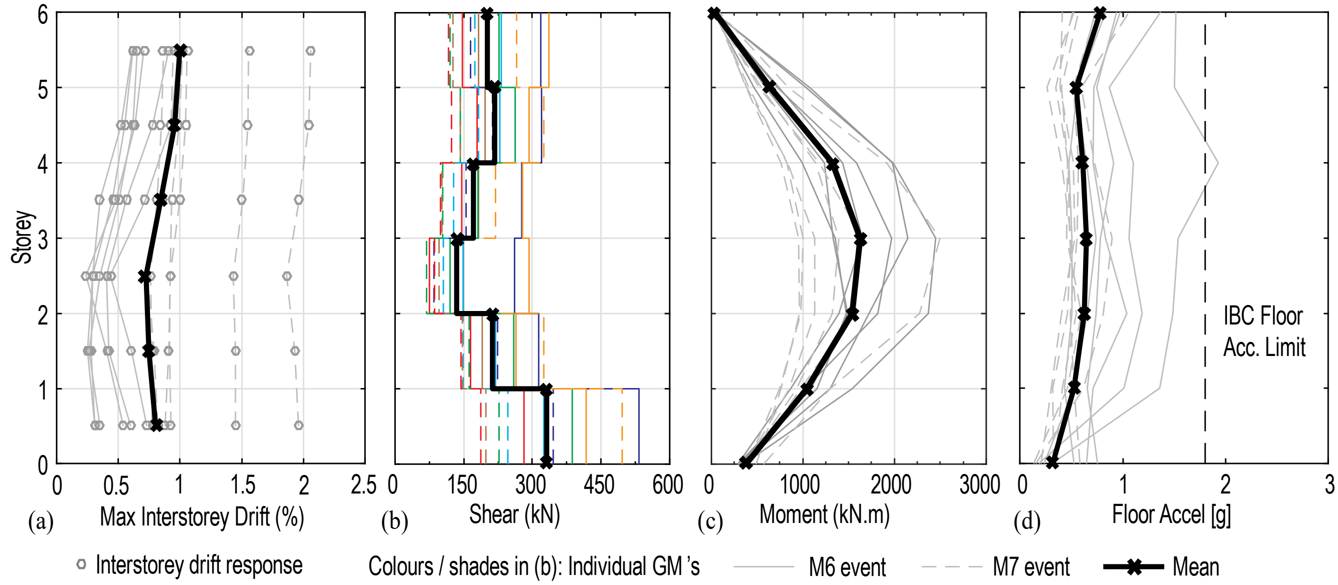

Fig. 4.2 – Response to all GMs: (a) interstorey drift; (b) shear; (c) bending moment; (d) floor acceleration

4.1 Prediction of Higher Mode Effects

The predictions of both the dynamic method and CBA are presented in Fig. 4.3, superimposed on the NLTHA results for each of the twelve GMs and their mean. Both the dynamic method and CBA predictions are similar in shape to the mean NLTHA results. However, the CBA prediction generally underestimates the NLTHA results in the upper half of the wall by as much as 30%, whereas the dynamic method generally matches the NLTHA results at the top of the wall and overestimates by no more than 15% in the bottom half.

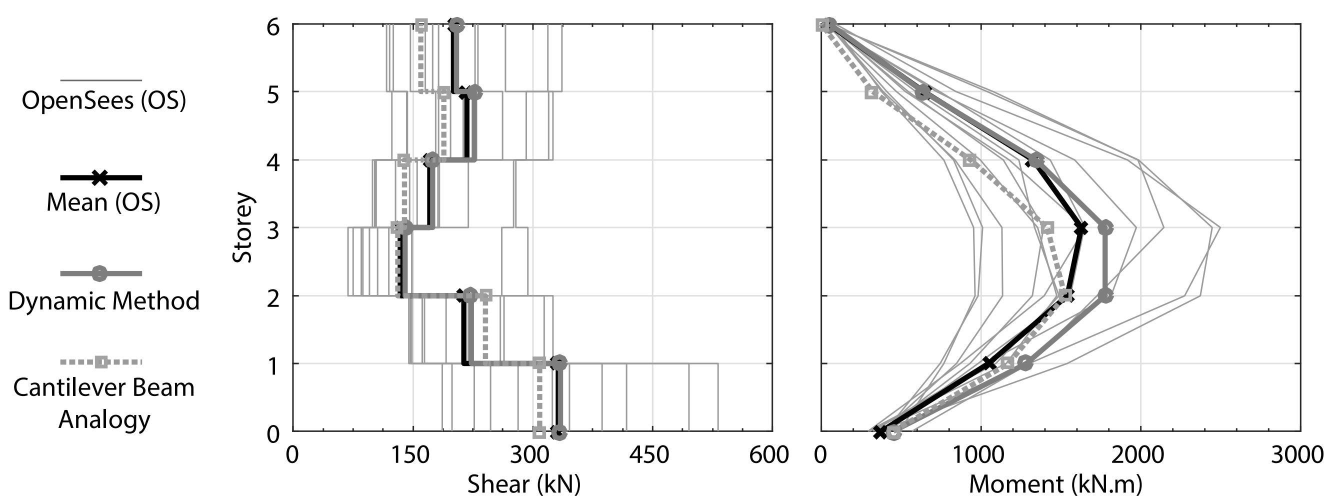

Fig. 4.3 – Comparison of shear and bending moment demands from NLTHA, dynamic method, and CBA

5. Conclusions

This paper investigated the performance of a simplified controlled rocking heavy timber wall (CRHTW) made of cross-laminated timber (CLT) subjected to low-to-moderate seismic demands. The wall was simplified by omitting supplemental energy dissipation and designing with a relatively large force reduction factor (R_dR_o = 8.0), thereby reducing the PT forces in order to avoid long-term timber creep. A six-storey prototype wall was designed for the low-to-moderate seismic hazard region of Ottawa, Canada. In addition to reviewing the analysis and design process, the effects of the higher modes on the peak shears and bending moments were estimated for the prototype using recently proposed techniques.

Based on non-linear time history analysis (NLTHA), the interstorey drifts were below the 2.5% limit for normal importance buildings in the Canadian building code [18], and the floor accelerations were significantly below the 1.8 g limit suggested for non-structural performance [27]. However, both these parameters and the force demand envelopes demonstrated influences from higher modes over the height of the structure. The maximum demands were 28% and 35% of the bending moment and shear capacity, respectively. These ratios do not require changes to the CRHTW design, but the bending moment and shear envelopes over the height of the structure demonstrate the significant increase in demand relative to the equivalent static force procedure demands determined during the initial base connection analysis and design stages.

The results of two higher mode prediction methods were compared with the NLTHA results. The dynamic method enveloped the NLTHA results, with a maximum 15% overestimation in the lower half of the structure. In contrast, the cantilever beam analogy had a similar shape and matched the NLTHA results in the lower half of the structure, but it underestimated the NLTHA results by as much as 30% in the top half of the structure. Further research is needed to determine whether similar agreement can be expected for other CRHTW designs in which supplemental energy dissipation has been omitted.

Although the CLT CRHTW strength capacities were found to be adequate for the demand in this study, timber engineers are still studying the capacity of CLT. The in-plane shear and bending strength and stiffness values used in the capacity calculation are based on recent research on small-scale specimens [28], such as beams and lintels. Additional research is required to verify the performance of larger scale specimens like the nine-layer, 2.44 m wide wall specified in the CRHTW design. For designs where the strength capacity does not meet the demand, the CRHTW could possibly incorporate higher mode mitigation techniques like multiple rocking sections [7,23].

6. Acknowledgements

The research presented in this paper was supported by the Ontario Graduate Scholarship (OGS) and by the NSERC Discovery Grant program.

7. References

[1] P. Blaikie, T. Cannon, I. Davis, and B. Wisner, *At Risk: Natural Hazards, People's Vulnerability and Disasters*, Second Edi. Oxon, United Kingdon: Routledge, 2003.

[2] H. W. Fischer III, C. K. Scharnberger, and C. J. Geiger, "Reducing seismic vulnerability in low to moderate risk areas," *Disaster Prev. Manag.*, vol. 5, no. 4, p. 5, 1996.

[3] Natural Resources Canada, "The Potential of Cross Laminated Timber in North American Construction," *Canadian Forest Service Spotlight*, 2013. [Online]. Available: http://publications.gc.ca/collections/collection_2013/rncan-nrcan/Fo12-44-2013-1-eng.pdf. [Accessed: 08-Apr-2015].

[4] A. Polastri, L. Pozza, C. Loss, and I. Smith, "Numerical analyses of high- and medium-rise CLT buildings braced with cores and additional shear walls," in *Structures and Architecture*, CRC Press, 2016, pp. 128–136.

[5] A. H. Buchanan, B. Deam, M. Fragiacomo, S. Pampanin, and A. Palermo, "Multi-Storey Prestressed Timber Buildings in New Zealand," *Struct. Eng. Int.*, vol. 18, no. 2, pp. 166–173, May 2008.

[6] C. Dickof, "CLT infill panels in steel moment resisting frames as a hybrid seismic force resisting system," University of British Columbia, 2013.

[7] R. S. Ganey, "Seismic Design and Testing of Rocking Cross Laminated Timber Walls," Master of Science, University of Washington, 2015.

[8] A. Palermo, S. Pampanin, A. H. Buchanan, and M. P. Newcombe, "Seismic design of multi-storey buildings using laminated veneer lumber (LVL)," in *New Zealand Society of Earthquake Engineering Conference*, 2005.

[9] F. Sarti, "Seismic Design of Low-Damage Post-Tensioned Timber Wall Systems," Doctor of Philosophy, University of Canterbury, 2015.
[10] M. P. Newcombe, "Seismic Design of Post-Tensioned Timber Frame and Wall Buildings," Doctor of Philosophy, University of Canterbury, 2011.
[11] KLH UK, "Technical," 2015. [Online]. Available: http://www.klhuk.com/product-/technical.aspx. [Accessed: 25-Sep-2015].
[12] Nordic Structures, "Nordic X-LAM Cross-Laminated Timber (CLT)," 2015. [Online]. Available: http://nordic.ca/en/products/nordic-x-lam-cross-laminated-timber-clt. [Accessed: 25-Sep-2015].
[13] S. Gagnon and C. Pirvu, *CLT Handbook*, Canadian E. Quebec City, Quebec: FPInnovations, 2011.
[14] M. Kovacs, "Seismic Design of Controlled Rocking Heavy Timber in a Low-to-Moderate Seismic Context," McMaster University, 2016.
[15] DSI, "DYWIDAG Post-Tensioning System using Bars." DYWIDAG Systems International, 2015.
[16] M. Kovacs and L. Wiebe, "Seismic Design of Heavy Timber in Low-to-Moderate Seismic Hazard Regions," McMaster University, Hamilton, Ontario, 2016.
[17] A. B. Robertson, "A Comparative Life Cycle Assessment of Mid-Rise Office Building Construction Alternatives: Laminated Timber Or Reinforced Concrete," Masters of Applied Science, University of British Columbia, 2011.
[18] NRCC, *National Building Code of Canada - Chapter 4*. Canadian Commission on Building and Fire Codes, 2010.
[19] M. P. Newcombe, "The Connection Response of Rocking Timber Walls," *SESOC J.*, vol. 28, no. 1, pp. 46–53, 2015.
[20] L. Wiebe and C. Christopoulos, "Performance-Based Seismic Design of Controlled Rocking Steel Braced Frames. I: Methodological Framework and Design of Base Rocking Joint," *J. Struct. Eng.*, vol. 141, no. 9, p. 04014226, 2015.
[21] C. Zhang, "Seismic Displacement Demands On Self-Centering Single-Degree-of-Freedom Systems," Master of Applied Science, McMaster University, 2015.
[22] T. C. Steele and L. D. A. Wiebe, "Dynamic and equivalent static procedures for capacity design of controlled rocking steel braced frames," *Earthq. Eng. Struct. Dyn.*, vol. in press, 2016.
[23] L. Wiebe and C. Christopoulos, "Performance-Based Seismic Design of Controlled Rocking Steel Braced Frames. II: Design of Capacity-Protected Elements," *J. Struct. Eng.*, vol. 141, no. 9, p. 04014227, 2015.
[24] S. Mazzoni, F. McKenna, M. H. Scott, and G. L. Fenves, *OpenSees Command Language Manual*. Berkeley, California: Pacific Earthquake Engineering Research (PEER) Center, 2006.
[25] G. M. Atkinson, "Earthquake time histories compatible with the 2005 National building code of Canada uniform hazard spectrum," *Can. J. Civ. Eng.*, vol. 36, no. 6, pp. 991–1000, Jun. 2009.
[26] G. M. Atkinson, N. Bouaanani, P. Daneshvar, S. Koboevic, P. Léger, and R. Tremblay, "Selection and scaling of ground motion time histories for seismic analysis using NBCC 2015," in *Canadian Conference on Earthquake Engineering*, 2015.
[27] M. A. Rahman and S. Sritharan, "Seismic response of precast, posttensioned concrete jointed wall systems designed for low- to midrise buildings using the direct displacement-based approach," *PCI J.*, no. March-April, pp. 38–56, 2015.
[28] S. Gagnon, M. Mohammad, W. M. Toro, and M. Popovski, "Evaluation of In-Plane Shear Strength of CLT," in *World Conference on Timber Engineering*, 2014, no. November, pp. 1–7.